Design and Experimental Validation of an Embedded Sliding Mode Controller for Voltage Regulation With SEPIC Converters

Gianmario Rinaldi, Prathyush P Menon, and Antonella Ferrara, *Fellow, IEEE*

***Abstract*—This article addresses the challenge of regulating the output voltage in single-end primary inductor converters (SEPICs) and introduces a practical solution based on the generation of second-order suboptimal sliding modes (2-SOSM). In contrast to the common assumption of a lossless SEPIC, in this article, a lossy SEPIC is explored. A concise mathematical representation of its model is presented, and the equilibrium point is explicitly defined. Using only the output voltage as a measurement, it is proven that the proposed 2-SOSM strategy achieves finite-time convergence of the output voltage with its reference. The proposed method effectively handles saturation constraints on the control variable, ensuring that the SEPIC duty ratio remains between 0 and 1. Furthermore, the approach proves to be robust to variations in the load resistor. The experimental analysis validates the effectiveness of our proposal and highlights its practical benefits. A comparison with a standard proportional integral control on an embedded platform underscores the superiority of the adopted approach.**

***Index Terms*—Control systems, dc–dc converter, nonlinear dynamics, robust control, voltage control.**

I. Introduction

A. Research Background

DC–DC converters are becoming popular devices in a wide range of applications, such as smart grids [1], [2], photovoltaic arrays for electric power generation [3], lithium-ion batteries charging for electric vehicles [4], and also in fully electric zero-emission powertrains [5]. DC–DC converters generate an output dc voltage that can differ from the input dc voltage they receive [6]. The presence of electrical energy storage elements, such as capacitors and inductors, which are interconnected in a suitable way with switches, makes the voltage regulation process possible [7]. Amongst various typologies for dc–dc converters, the single-end primary inductor converter (SEPIC) has recently captured the attention of researchers and practitioners [8], [9], [10]. The SEPIC is capable of generating a wide range of output voltages that can be lower, equal, or higher than the input voltage, and therefore exhibits the so-called Buck–Boost behavior [6]. In addition, the SEPIC has the capability to reduce the current ripple during the switching phases, thus ensuring better performance compared to other types of converters [11].

Manuscript received 19 February 2024; revised 13 May 2024; accepted 8 June 2024. Date of publication 19 June 2024; date of current version 16 July 2024. This work was supported in part by the Innovate U.K. Project CMDC Twin Motor, Zero Emission Powertrain For Commercial Workboats with Ecomar Propulsion Ltd. under Grant 10005693 TS/W012197/1. Recommended for publication by Associate Editor Y. Yan. *(Corresponding author: Gianmario Rinaldi.)*

Gianmario Rinaldi and Prathyush P Menon are with the Department of Engineering, Faculty of Environment, Science and Economy (ESE), University of Exeter, EX4 4QF Exeter, U.K. (e-mail: G.Rinaldi3@exeter.ac.uk; P.M.Prathyush@exeter.ac.uk).

Antonella Ferrara is with the Department of Electrical, Computer and Biomedical Engineering, University of Pavia, 27100 Pavia, Italy (e-mail: antonella.ferrara@unipv.it).

Color versions of one or more figures in this article are available at https://doi.org/10.1109/TPEL.2024.3415164.

Digital Object Identifier 10.1109/TPEL.2024.3415164

B. Literature Review

A number of solutions have been proposed to regulate the current and the output voltage for SEPICs. To design a control law, it is conventionally assumed that the SEPIC operates in continuous conduction mode (CCM) (which means that the currents never nullify) [12]. In [13], a model predictive control (MPC) technique has been proposed to control the SEPIC current of inductors. The method relied on several sensors for the implementation of the control algorithm. In [14], conventional proportional-integral-derivative (PID) and PI-like fuzzy control architectures were compared considering as a show case the control of a SEPIC output voltage to power a solar-fed pump for irrigation. Other solutions were inspired by passivity-based techniques such as in [15], where a control law expression is derived depending on the voltages and currents of the SEPIC, and more recently in [16], where a linear matrix inequality problem has been solved and a cascade control architecture has been exploited to ensure faster asymptotic output voltage tracking. More recently, in [8], it has been proven that a direct voltage regulation requiring only the output voltage measurement is possible for SEPICs, and rules to design higher order controllers were outlined and tested.

Sliding mode (SM) control techniques have been successfully applied to control electrical devices in microgrids and energy networks [17], [18]. SM control schemes are well known to be robust to input disturbances and to be able to enforce a *finite time* stabilization of the controlled systems [19]. Several SM-based control strategies have been proposed for dc–dc converters, including SEPICs [20], [21], [22]. First-order SM (1-SM) controllers are discontinous algorithms designed to drive system states to a predefined sliding surface and maintain them there, achieving robust performance against disturbances [19]. Once the state of the system reaches the sliding surface, the 1-SM law ensures that the states remain on this surface, achieving

the desired behavior of the system with a discontinuous control action. This results in a chattering phenomenon due to high-frequency switching of the control input [23]. Second-order SM controllers (2-SM) extend this principle, aiming to reduce chattering through smoother control actions and enhanced precision, by acting on higher derivatives of the sliding variable, thus offering improved robustness and dynamic response [18], [19], [24]. In order to design a SM controller, the relative degree should be known. The relative degree is defined as the number of times you need to differentiate the output to get an expression that explicitly includes the control input [19].

Conventionally, the control variable for dc–dc converters regulated using SM techniques has been selected as the binary signal of the switch that can assume only *two* values $\{0, 1\}$ [18], [21]. (The value 1 imposes that the switch is ON, while the value 0 imposes that it is OFF). This approach is named *Conventional Hysteresis-Modulation (HM)*-Based SM Controller, and is based on the switched dynamics of the converters. HM-based controllers are easy to implement, but require a fixed (and high) sampling frequency to be practically implemented [25]. To overcome this issue, a *Pulsewidth-Modulation (PWM)*-Based SM controller has been suggested [25], [26]. The PWM-based SM approach is designed based on an averaged dynamical model per cycle of the SEPIC [27]. This approach aims to determine a *smooth* control variable that can assume *any* value between $[0, 1]$ (see, for example, [22], [28]). Therefore, the control variable represents the well-known *duty ratio*, which is the fraction of the duty cycle during which the switch is maintained ON [27]. Mamarelis et al. [29] investigated severalHM-based SM control solutions to achieve maximum power point tracking of photovoltaic power sources coupled with SEPICs. A novel HM-based SM control law was explored in [30], where an optimization method was used to synthesise the controller parameters ensuring better tracking performances. In [12], an indirect HM-based SM voltage regulation was achieved by coupling a standard PI controller with a 1-SM controller. In [31], a linear combination of the four state variables of the SEPIC was chosen as the sliding surface and the performance of the controller was experimentally validated via hardware in the loop (HIL). The approach required the implementation of a significant number of sensors.

Relatively little attention has been paid so far in the literature to designing PWM-based SM control algorithms. For example, in [11], a discrete time implementation of a PWM-based SM control scheme were undertaken in [11], along with a small signal linearization approach to analyse the stability properties of the controlled device. An interesting PWM-based SM control approach was conceived by [26], where the SEPIC feeds a constant power load, and the sliding variable was chosen as the power setting point. Differently, in [32], a PWM-based SM controller was designed to regulate both the output voltage and the inductor current, requiring two sensors to be implemented.

C. Main Contribution

This article proposes and experimentally validates a novel PMW-based SM technique to regulate *in finite time* the output voltage for SEPICs operating in CCM. Most of the work in the literature assumed that SEPICs were lossless [12], [21]. To be more consistent with the real data sheets of the SEPICs [33], [34], in the present work, this first assumption is relaxed, considering the presence of lossy inductors in the circuit. An original compact mathematical representation of the SEPICs dynamic is derived along with the explicit representation of its equilibrium point. To the best of our knowledge, the only PWM-based strategy addressing direct voltage regulation for SEPIC has recently been proposed in [8]. This methodology was characterised by an *asymptotic* converge of the output voltage to its set point. Similarly to [8], the hardware cost and complexity of the sensor network can be shown to be reduced by only acquiring the output voltage of the SEPIC. But distinctively from the existing solution mentioned above, in this article the suboptimal sliding mode (2-SOSM) principle is exploited to ensure a finite time voltage regulation. More precisely, inspired by a recent 2-SOSM technique proposed by Ferrara and Rubagotti [35], a control law determining the duty ratio for the PWM modulation of the MOSFET of SEPICs is designed. The present proposal is able to solve *in finite time* the voltage regulation problem, while simultaneously ensuring that the control variable always remains within the interval value $(0, 1)$. This guarantees that the proposed methodology is characterized by interesting and faster performances compared to existing solutions characterised by *asymptotic* convergence, such as [8], [13], [15]. In addition, by virtue of the use of 2-SOSM, applied to a system that exhibits a relative degree *one* property [19], the generation of a *continuous* control signal for PWM modulation can be ensured. The hypothesis of the article is tested through a real-time experiment conducted on an embedded system with the SEPIC kit *TMDCDCLEDKIT* [34]. The chosen experimental set-up included a PI control strategy already developed by device makers to achieve voltage regulation for the SEPIC. The performance of our 2-SOSM controller is compared with the existing PI controller of the manufacturer to show that our proposal can provide a remarkable performance improvement for voltage regulation and tracking.

TABLE I
COMPARISON OF DIFFERENT CONTROL ALGORITHMS FOR SEPIC VOLTAGE REGULATION

Algorithm:	Rel. Degree	Sat.	Chattering	Deriv.	Score
PID	1	✗	mitigated	σ, $\dot{\sigma}$	1
1-SM	1	✓	present	σ	2
STA	1	✗	mitigated	σ	2
Other 2-SM	1, 2	✗	mitigated	σ, $\dot{\sigma}$	2
2-SOSM	1, 2	✗	mitigated	σ	3
2-SOSM+SAT	1, 2	✓	mitigated	σ	4

To further justify the advantages of the proposal of this article, Table I provides a comparative analysis of different control algorithms applied to the regulation of the SEPIC output voltage. It assesses six distinct algorithms: PID, 1-SM, Sliding Mode Super-Twisting Algorithm (STA), 2-SM, the conventional second order sub optimal sliding mode (2-SOSM), and the proposal adopted in this article, which is called (2-SOSM+SAT). The analysis is based on four criteria, which are: the relative degree between the output and input, the ability of the algorithm to manage the input saturation constraints, its effectiveness in

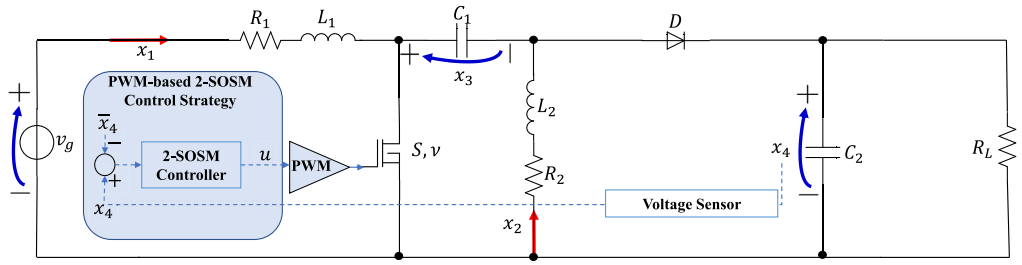

State Variables and Input Signals		
x_1	(A)	Current through the inductor (R_1, L_1)
x_2	(A)	Current through the inductor (R_2, L_2)
x_3	(V)	Voltage of C_1
x_4	(V)	Voltage of C_2
v_g	(V)	Input voltage source
ν	(-)	Switch S status, $\nu = 1$, ON, $\nu = 0$, OFF
u	(-)	PWM modulation control signal (duty ratio)
		Voltage difference (V)
		Current (A)

Model Parameters and Symbols		
$L_1 = 470$	(μH)	First inductor value
$L_2 = 330$	(μH)	Second inductor value
$R_1 = 280$	($m\Omega$)	First inductor resistance
$R_2 = 230$	($m\Omega$)	Second inductor resistance
$C_1 = 470$	(μF)	Second capacitor value
$C_2 = 470$	(μF)	Second capacitor value
$R_L = 1$	(kΩ)	Load resistor
S	(-)	MOSFET switch
D	(-)	Diode

Fig. 1. SEPIC topology along with the definition of the state variables, the input signals, the model parameters, and symbols. Arrowheads indicate the positive currents and voltages sign convention. The values of the model parameters are taken directly from the real data sheet in [33] and [34].

mitigating chattering effects, and whether the algorithm requires knowledge of the time derivative $\dot{\sigma}$ of the output σ. The PID control displays a relative degree of one, fails to handle saturation, mitigates chattering, and requires knowledge of both the output and its rate of change, scoring the lowest at 1. The 1-SM and STA have similar characteristics but do not require knowledge of the rate of change, scoring 2. The other 2-SM can handle systems of relative degree 1 and 2, mitigates chattering, but needs knowledge of the output rate of change, also scoring 2. The SOSM method, like "Other 2-SM," manages chattering and requires only the output knowledge, scoring 3. The highest score of 4 is awarded to algorithm adopted in this article, which successfully handles saturation, mitigates chattering, and only needs the output σ, not its derivative $\dot{\sigma}$.

Notation: The notation used in the article is standard. For a scalar signal x, $\text{sign}(x)$ denotes its sign function, while $|x|$ denotes its absolute value. For a vector or matrix X, $X^\top$ denotes its transpose, while $||X||$ denotes its Euclidean norm. The symbol $\text{Diag}(x_1, x_2, \ldots, x_n)$ represents a diagonal matrix with its diagonal entries. For a variable or time-varying parameter x, the symbol $\overline{x}$ denotes a specific constant value of x.

Structure of the Article: The rest of this article is organized as follows. In Section II, the SEPIC dynamical model is introduced. Section III presents the design of the proposed control scheme and the stability analysis. Section IV discusses the experiments undertaken to validate our proposal. Finally, Section V concludes this article.

II. System Description

The circuit diagram of the SEPIC is shown in Fig. 1. SEPIC is a switched dc–dc power converter, which can have an output voltage greater than, less than or equal to the input voltage, which means that it exhibits the so-called buck–boost behavior [6]. The SEPIC circuit is composed of two lossy inductors modeled by pairs (L_1, R_1) and (L_2, R_2), two capacitors C_1 and C_2, the diode D, the MOSFET S and the load equivalent resistance R_L [7]. The state variables, denoted as $x \in \mathbb{R}^4$, comprise the inductor currents (x_1 and x_2) and the capacitor voltages (x_3 and x_4), as indicated in Fig. 1. The SEPIC is powered by a constant dc input voltage power source v_g, and the state x_4, i.e., the voltage of C_2 and the load R_L, denotes the only available measured output. Let $\nu : \mathbb{R} \to \{0, 1\}$ be a switching function indicating the state of the MOSFET switch S at any instant t. Furthermore, let the operating switching frequency be assumed to be fixed at $f_\nu := 1/T_\nu$. The SEPIC can operate in two distinct modes, which are: *Mode 1* (MOSFET is "ON," i.e., $\nu = 1$) and *Mode 2* (MOSFET is "OFF," i.e., $\nu = 0$).

Mode 1

During ***Mode 1***, the MOSFET S is switched ON. In such a situation, the diode D is reverse biased, open, and conducting no current. The current in the first inductor x_1 increases exponentially. The capacitor C_1 provides the energy to the inductor (L_2, R_2), while the capacitor C_2 discharges its energy on the load R_L. The state-space representation for Mode 1 yields

$$\left.\begin{array}{l} E\dot{x} = (A_1 - R)x + Bv_g \end{array}\right\} \begin{array}{c} \textbf{Mode 1} \\ \text{S-ON}, \nu = 1 \end{array} \tag{1}$$

where: $E = \text{Diag}(L_1, L_2, C_1, C_2)$, $R = \text{Diag}(R_1, R_2, 0, 1/R_L)$, $B = [1/L_1, 0, 0, 0]^\top$. Matrix

$$A_1 = \begin{bmatrix} 0 & 0 & 0 & 0 \\ 0 & 0 & 1 & 0 \\ 0 & -1 & 0 & 0 \\ 0 & 0 & 0 & 0 \end{bmatrix}$$

is skew-symmetric and independent of the model parameters of the SEPIC. It represents the power exchanges throughout the circuit. Note that the matrix E is invertible and that matrix $(A_1 - R)$ can be shown to be Hurwitz by direct calculation.

Mode 2

During ***Mode 2***, the MOSFET is switched OFF. In this situation, diode D can conduct the current. The energy stored in the two inductors discharges through the capacitors C_1 and C_2 and the load R_L. The state-space representation for Mode 2 yields

$$E\dot{x} = (A_2 - R)x + Bv_g \Big\} \begin{array}{c} \text{Mode 2} \\ \text{S-OFF}, \nu = 0 \end{array} \tag{2}$$

where matrix A_2

$$A_2 = \begin{bmatrix} 0 & 0 & -1 & -1 \\ 0 & 0 & 0 & -1 \\ 1 & 0 & 0 & 0 \\ 1 & 1 & 0 & 0 \end{bmatrix}$$

is again skew-symmetric and independent of the model parameters of the SEPIC but it represents the power exchanges throughout the circuit. Note that the matrix $(A_2 - R)$ can be shown to be Hurwitz by direct calculation.

State Space Averaging Model

Suppose that the duration of the duty cycle of the SEPIC is set equal to T_ν seconds, and assume that for $T_d < T_\nu$ seconds, the MOSFET S is ON ($\nu = 1$), while for the remaining $T_d' = T_\nu - T_d$ seconds the MOSFET S is OFF ($\nu = 0$). Define the duty ratio $u := T_d/T_\nu$. The variable u practically represents the percentage of the duty cycle (expressed in units value between 0 and 1) during which the MOSFET remains in Mode 1, and coincides with the averaged switching control input u for MOSFET PWM modulation [36]. The state-space averaging technique aims to replace the state-space representations (1) and (2) of the two successive phases of the switching cycle T_ν with a *single* state-space description that represents approximately the behavior of the SEPIC during the whole period of duration T_ν. The approach consists in summing up the right-hand side of (1) multiplied by u and the right-hand side of (2) multiplied by $(1 - u)$, which yields [6]

$$E\dot{x} = [uA_1 + (1 - u)A_2 - R]x + Bv_g \tag{3}$$

$$y = Cx. \tag{4}$$

In (4), the output equation is introduced, where $C = [0,\ 0,\ 0,\ 1]$, as it is assumed to only measure the value of the voltage at the capacitor C_2, which coincides with the voltage at the load terminals.

III. Controller Design

The control objective to address is:

Objective 1 (Voltage Regulation): Given a constant voltage reference $\overline{y} := \overline{x}_4$, it is necessary to ensure

$$y = \overline{y} \tag{5}$$

in finite time, where $\overline{x}_4$ is a positive known constant expressed in Volts.

Remark 1 (Voltage Reference): The reference output voltage $\overline{x}_4$ is considered to be constant to theoretically analyse the equilibrium point and the stability property of the SEPIC system. However, in the embedded experiments presented in Section IV, the performances of the proposed controller under time-varying voltage reference will be investigated. In the literature, it is also conventional to relax certain assumptions (instrumental exclusively for mathematical stability analysis), in simulations or real experiments, to test the performance of the controllers [22]. The observed efficacy under time-varying voltage reference is attributed to the inherent robustness of the adopted 2-SOSM control algorithm, which will be shown to be totally insensitive to such variations.

To solve Objective 1, three assumptions are introduced:

Assumption 1: It is assumed that

A1) The system parameters L_1, L_2, R_1, R_2, C_1, C_2, and R_L are *unknown* but constant with known bounds.

A2) The SEPIC always operates in *CCM* [6], which implies that the currents always satisfy $x_1 > 0$ and $x_2 > 0$, and they remain bounded along with their first time derivatives, i.e., $x_1 < \Delta_{1_{x_1}}$, $x_2 < \Delta_{1_{x_2}}$, $\dot{x}_1 < \Delta_{2_{x_1}}$, $\dot{x}_2 < \Delta_{2_{x_2}}$ where $\Delta_{1_{x_1}}$, $\Delta_{1_{x_2}}$, $\Delta_{2_{x_1}}$, $\Delta_{2_{x_2}}$ are known positive constants.

A3) The voltage source v_g and the voltage level at the load terminals x_4 always remain positive.

Remark 2 (Assumption 1 Rationals): Assumption 1-(A1) requires that only the bounds of the SEPIC parameters L_1, L_2, R_1, R_2, C_1, C_2 and R_L are known, not their exact numerical values. This allows the proposed solution to be easily adaptable to SEPICs of different sizes and power. Assumption 1-(A2) has been commonly adopted in many relevant solutions (see, e.g., [8], [12]). Due to the presence of lossy inductors in the circuit, it is also reasonable to assume that their associated currents and their first time derivatives remain bounded with known upper limits. These bounds can be tuned from an engineering understanding of the circuit. Assumption 1-(A3) prescribes no change of polarities in the input v_g and output x_4 voltages, and is generally satisfied in many practical cases [6].

A. Steady-State Behavior

The steady-state representations of the state variables can be calculated for a constant control input $\overline{u}$, satisfying $0 < \overline{u} < 1$. An explicit solution exists for the equilibrium values of the state variables and is unique. By imposing

$$[\overline{u}A_1 + (1 - \overline{u})A_2 - R]\overline{x} + Bv_g = 0 \tag{6}$$

from (3), after straightforward algebraic manipulations, the explicit solution of the constant state vector $\overline{x} := [\overline{x}_1,\ \overline{x}_2,\ \overline{x}_3,\ \overline{x}_4]^T$ is obtained as

$$\overline{x}_1 = \frac{1}{R_L}\left(\frac{\overline{u}}{1 - \overline{u}}\right)\overline{x}_4 \tag{7}$$

$$\overline{x}_2 = \frac{\overline{x}_4}{R_L} \tag{8}$$

$$\overline{x}_3 = \left(\frac{R_2}{\overline{u}R_L} + \frac{1-\overline{u}}{\overline{u}}\right)\overline{x}_4 \tag{9}$$

$$\overline{x}_4 = \left(\frac{\overline{u}}{1-\overline{u}} + \frac{1}{R_L}\left(\frac{1-\overline{u}}{\overline{u}}R_2 + \frac{\overline{u}}{1-\overline{u}}R_1\right)\right)v_g. \tag{10}$$

Remark 3 (Lossless SEPIC): If the two inductors of the SEPIC are assumed lossless, it follows that $R_1 = 0$ and $R_2 = 0$. In such a situation, the equilibrium solution (7)–(10) can be simplified as

$$\overline{x}_1 = \frac{1}{R_L}\left(\frac{\overline{u}}{1-\overline{u}}\right)\overline{x}_4 \tag{11}$$

$$\overline{x}_2 = \frac{\overline{x}_4}{R_L} \tag{12}$$

$$\overline{x}_3 = \left(\frac{1-\overline{u}}{\overline{u}}\right)\overline{x}_4 = v_g \tag{13}$$

$$\overline{x}_4 = \left(\frac{\overline{u}}{1-\overline{u}}\right)v_g. \tag{14}$$

The solution reported in (11)–(14) is the typical representation of the equilibrium solution for lossless SEPICs determined in the existing literature [12].

B. Closed Loop Control and Stability Analysis

In Section III-A, it has been shown that for a given constant value of the control input $\overline{u}$ (the duty ratio), there is a unique equilibrium point for SEPIC according to the system (7)–(10). In this section, the problem defined in Objective 1 is solved in two steps: 1) First, a 2-SOSM is proven to be enforced *in finite time*, ensuring $x_4 = \overline{x}_4$; 2) A stability analysis is undertaken once the sliding mode is attained, formally proving that also the other three states x_1, x_2, x_3 in (7)–(9) reach their equilibrium values asymptotically. To attain the control Objective 1, the error variable σ is defined as $\sigma := y - \overline{y}$ which has to be nullified in finite time. The following control scheme is proposed:

PWM-based SM Controlled system:

$$E\dot{x} = [uA_1 + (1-u)A_2 - R]x + Bv_g \tag{15}$$

$$y = Cx. \tag{16}$$

Control Scheme:

$$\sigma := y - \overline{y} \tag{17}$$

$$u := \frac{1}{2}(1 - u_{\text{sm}}) \tag{18}$$

$$\dot{u}_{\text{sm}} = w_{\text{sm}} \tag{19}$$

$$w_{\text{sm}} = \begin{cases} -\alpha\mu\text{sign}(\sigma - \beta\sigma_M) & \text{if } |u_{\text{sm}}| < 1 \\ -\mu\text{sign}(u_{\text{sm}}) & \text{else} \end{cases} \tag{20}$$

where the auxiliary signals u_{sm}, w_{sm} govern the evolution of the duty ration u, and μ is a positive constant to be designed. The variable σ_M represents the last extremal value of σ. The variables α, β are time-varying parameters that will be defined in the sequel. The control scheme proposed here is inspired by the 2-SOM methodology developed in [35]. The desaturation principles provided by (20) are introduced to ensure that the control signal u always remains between 0 and 1 [35].

Lemma 1: Consider the controlled SEPIC dynamical model (15)–(20). Under Assumption 1, the condition

$$|u_{\text{sm}}| < 1 \tag{21}$$

holds if the sliding mode is attained, e.g., when $\sigma = \dot{\sigma} = 0$.

Proof: The first time derivative of the sliding variable σ is

$$\dot{\sigma} = \dot{x}_4$$

$$\dot{\sigma} = (1-u)\frac{x_1 + x_2}{C_2} - \frac{1}{R_L C_2}x_4. \tag{22}$$

By imposing $\dot{\sigma} = 0$, an explicit expressions for u yields

$$u = 1 - \frac{\overline{x}_4}{R_L(x_1 + x_2)}. \tag{23}$$

Note that from (23), as $0 < u < 1$, during the sliding mode the current absorbed by the load $(\overline{x}_4/R_L)$ (which is a constant) is strictly smaller than the sum of the currents in the two inductors $(x_1 + x_2)$, i.e.,

$$\left.\frac{\overline{x}_4}{R_L} < x_1 + x_2\right\} \text{ as } 0 < u < 1. \tag{24}$$

As the signal u is defined by (18), the identity

$$1 - u = \frac{1}{2} + \frac{1}{2}u_{\text{sm}} \tag{25}$$

holds. By using (25), the expression for $\dot{\sigma}$ in (22) can be rewritten by making u_{sm} explicitly appear as

$$\dot{\sigma} = f(x) + g(x)u_{\text{sm}} \tag{26}$$

where the auxiliary functions $f(x)$ and $g(x)$ are

$$f(x) := \frac{x_1 + x_2}{2C_2} - \frac{1}{R_L C_2}x_4 \tag{27}$$

$$g(x) := \frac{x_1 + x_2}{2C_2}. \tag{28}$$

When the condition $\dot{\sigma} = 0$ is enforced, it is possible to determine the expression of the so-called equivalent control $u_{\text{sm}}^{\text{eq}}$ [18], [19], which is defined as

$$u_{\text{sm}}^{\text{eq}} = -\frac{f(x)}{g(x)} = -\frac{x_1 + x_2 - \dfrac{2\overline{x}_4}{R_L}}{x_1 + x_2}. \tag{29}$$

Under Assumption 1, the function $f(x)$ in (27) is always *bounded* which means

$$|f(x)| \le \frac{\Delta_{1_{x_1}} + \Delta_{1_{x_2}}}{2C_2} =: F \tag{30}$$

where F is a known positive constant. As $x_1 > 0$, $x_2 > 0$, it follows from the definition of $g(x)$ in (28) that

$$G_1 \le g(x) \le G_2 \tag{31}$$

where G_1 is an arbitrarily small positive constant, and G_2 satisfies

$$G_2 := \frac{\Delta_{1_{x_1}} + \Delta_{1_{x_2}}}{2C_2}. \tag{32}$$

From (27)–(28), and exploiting (30)–(31), and (24) it is guaranteed that

$$|f(x)| < g(x). \tag{33}$$

From (18) and (33), it follows that:

$$|u_{\text{sm}}^{\text{eq}}| = \frac{|f(x)|}{|g(x)|} < 1. \tag{34}$$

which proves the lemma. ■

Inspired by [19], [35], two variables are introduced: $\sigma_1 := \sigma$ and $\sigma_2 = \dot{\sigma}$, which evolves as

$$\dot{\sigma}_1 = f(x) + g(x)u_{\text{sm}} \tag{35}$$

$$\dot{\sigma}_2 = h(x, u_{\text{sm}}) + g(x)w_{\text{sm}} \tag{36}$$

where the function $h(x, u_{\text{sm}})$ is defined as

$$h(x, u_{\text{sm}}) = \dot{f}(x) + \dot{g}(x)u_{\text{sm}}. \tag{37}$$

Under Assumption 1, the function results in being a sum of bounded terms, hence $h(x, u_{\text{sm}})$ is bounded:

$$|h(x, u_{\text{sm}})| < H \tag{38}$$

where H is a known positive constant that can be shown to be governed by

$$H := \frac{\Delta_{2_{x_1}} + \Delta_{2_{x_2}}}{C_2}. \tag{39}$$

The time-varying parameters of the controller are governed by

$$\beta \in \left[\frac{1}{2},\, \beta_M\right] \tag{40}$$

$$\beta_M = \begin{cases} \frac{\sigma_1}{\sigma_M} & \text{if } |u_{\text{sm}}| > 1 \\ \frac{1}{2} & \text{if } \sigma_M \text{ changes or } t = 0 \end{cases} \tag{41}$$

$$\varphi := (\sigma_1 - \beta\sigma_M)(\sigma_M - \sigma_1) \tag{42}$$

$$\alpha = \begin{cases} \alpha^\star \in (0,\, 1] \cap (0, 3G_1/G_2), & \text{if } \varphi > 0 \\ 1 & \text{else} \end{cases} \tag{43}$$

$$\mu > \max\left(\frac{H}{\alpha^\star G_1};\, \frac{4H}{3G_1 - \alpha^\star G_2}\right). \tag{44}$$

Proposition 1: Under Assumption 1 and given Lemma 1,

A) Given the control scheme (18)–(20), with the associate parameters and variables (40)–(44), then the states of system (35)–(36) converge to the origin in a finite time T_v, satisfying Objective 1.
B) Once the sliding mode is attained, the control signal u_{sm} and therefore the duty ratio u remain constant.
C) The remaining states x_1, x_2, x_3 asymptotically reach their equilibrium values $\overline{x}_1$, $\overline{x}_2$, $\overline{x}_3$ (7)–(9).

Proof: The three parts of the proposition are proven in the order:

Proof of Part (A): Following the methodology in [35], it is possible to prove by means of the contraction properties that system (35)–(36) subject to the control action (18)–(20) converges to the origin in a finite time. This is achieved throughout the generation of a sequence of states ($\sigma_1 = \sigma_{M_i}$, $\sigma_2 = 0$), where

$$|\sigma_{M_{i+1}}| < |\sigma_{M_i}|. \tag{45}$$

The finite time T_v after which the condition $\sigma_1 = \sigma_2 = 0$ is attained is upper-bounded as follows [19], [35]:

$$T_v < \frac{(G_1 + \alpha^\star G_2\mu)}{(G_1\mu - H)\sqrt{\alpha^\star G_2\mu + H}} h(\sigma_1(0))\theta \tag{46}$$

where $h(\sigma_1(0))$ is a function of the initial condition of the sliding variable σ_1, and θ is a positive constant. Only by varying the design constant μ, it is apparent that $T_v \propto \frac{1}{\sqrt{\mu}}$, hence T_v can be reduced by increasing μ. Further details can be found in [35].

Proof of Part (B): To prove that the control signal u_{sm} remains constant during sliding mode, it is sufficient to expand the expression of $\dot{\sigma}_2$ and impose that it equal to 0

$$\dot{\sigma}_2 = (1 - u)\left(\frac{\dot{x}_1 + \dot{x}_2}{C_2}\right) - \frac{1}{2}w_{\text{sm}}\left(\frac{x_1 + x_2}{C_2}\right) = 0. \tag{47}$$

By defining $x_{12} := x_1 + x_2$, expanding (47) and multiplying the left and the right sides by the positive constant C_2, it yields

$$(1 - u)\dot{x}_{12} - \frac{1}{2}w_{\text{sm}}x_{12} = 0. \tag{48}$$

As $w_{\text{sm}} = 0$ during the sliding mode and $(1 - u) > 0$, it is possible to conclude from (48) that $\dot{x}_{12} = 0$, which guarantees that $x_{12} = x_1 + x_2$ is constant. From (23), it is immediate to see that u remains constant.

Proof of Part (C): Let us impose $x_4 = \overline{x}_4$ and consider u governed by (23) and being constant as per *Part (B)* of this proposition. The zero dynamics is derived

$$E_d\dot{x}_d = [\overline{u}A_{1\,d} + (1 - \overline{u})A_{2\,d} - R_d]x_d + B_dp_d \tag{49}$$

where the reduced-order vectors and matrices are $x_d = [x_1,\, x_2,\, x_3]^\top$, $E_d = \text{Diag}(L_1,\, L_2,\, C_1)$, $R = \text{Diag}(R_1,\, R_2,\, 0)$, $p_d = [v_g,\, \overline{x}_4]^\top$. Moreover, the matrices

$$B_d = \begin{bmatrix} 1 & -(1-\overline{u}) \\ 0 & -(1-\overline{u}) \\ 0 & 0 \end{bmatrix} A_{1\,d} = \begin{bmatrix} 0 & 0 & 0 \\ 0 & 0 & 1 \\ 0 & -1 & 0 \end{bmatrix}$$

$$A_{2\,d} = \begin{bmatrix} 0 & 0 & -1 \\ 0 & 0 & 0 \\ 1 & 0 & 0 \end{bmatrix}.$$

At the equilibrium (7)–(10), the algebraic condition

$$0 = [\overline{u}A_{1\,d} + (1 - \overline{u})A_{2\,d} - R_d]\overline{x}_d + B_dp_d \tag{50}$$

holds. If the error variable is defined as $\Delta x_d := x_d - \overline{x}_d$, and subtract (50) from (49) the error dynamics result in being

$$E_d\Delta\dot{x}_d = [\overline{u}A_{1\,d} + (1 - \overline{u})A_{2\,d} - R_d]\Delta x_d. \tag{51}$$

Matrix

$$M_d(\overline{u}) := E_d^{-1}[\overline{u}A_{1\,d} + (1 - \overline{u})A_{2\,d} - R_d]. \tag{52}$$

is adopted to compactly rewrite the error dynamics as

$$\Delta\dot{x}_d = M_d(\overline{u})\Delta x_d. \tag{53}$$

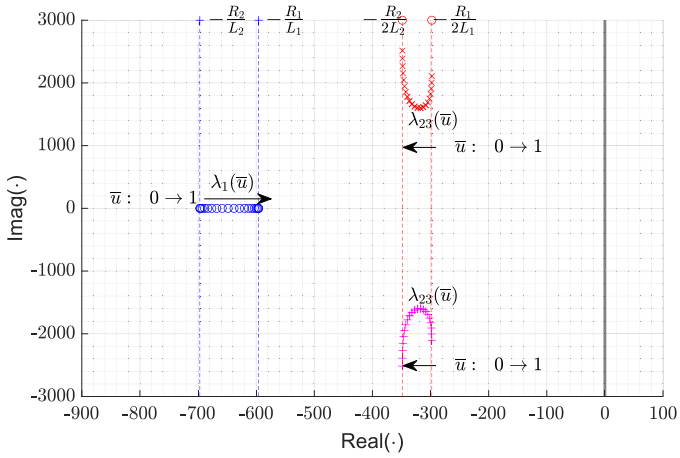

Fig. 2. Position of the eigenvalues $\lambda_1(\overline{u})$, $\lambda_{23}(\overline{u})$ on the complex plane. The arrow indicate the direction of movement of the eigenvalues when $\overline{u}$ increases from 0 to 1.

$M_d(\overline{u})$ for a fixed $\overline{u}$ is a constant matrix that can be shown to be Hurwitz. Consider the three eigenvalues $\lambda_1(\overline{u})$, $\lambda_{2,3}(\overline{u})$ of $M_d(\overline{u})$, where $\lambda_{2,3}(\overline{u})$ represents a complex conjugate pair. It is possible to show that

$$\lambda_1(\overline{u}=0) = -\frac{R_2}{L_2} \tag{54}$$

$$\lambda_{2,3}(\overline{u}=0) = -\frac{R_1}{2L_1} \pm \left(\frac{\sqrt{4L_1 - C_1R_1^2}}{2L_1\sqrt{C_1}}\right) j \tag{55}$$

hence $M_d(\overline{u}=0)$ is Hurwitz. If the analysis is repeated

$$\lambda_1(\overline{u}=1) = -\frac{R_1}{L_1} \tag{56}$$

$$\lambda_{2,3}(\overline{u}=1) = -\frac{R_2}{2L_2} \pm \left(\frac{\sqrt{4L_2 - C_1R_2^2}}{2L_2\sqrt{C_1}}\right) j. \tag{57}$$

It is possible to conclude that also $M_d(\overline{u}=1)$ is Hurwitz. The eigevanlues $\lambda_1(\overline{u})$, $\lambda_{2,3}(\overline{u})$ smoothly evolve from the set of values (54)–(55) to the values given in (56)–(57), as indicated in Fig. 2. It is possible to conclude that the constant matrix $M_d(\overline{u})$ is Hurwitz $\forall\, \overline{u} : 0 < \overline{u} < 1$, and x_d asymptotically converges to $\overline{x}_d$. ■

Remark 4 (Reaching Phase): In the stability analysis, in Part (B)–(C) of Proposition 1 it is proven that during the sliding phase (i.e., when $\sigma_1 = \sigma_2 = 0$ from (35)–(36)), the control variable u is constant, and the error system in (51) is asymptotically driven to the origin. The reaching phase is a finite-time transient that takes place only once. During this phase, the norm of the sliding variable $|\sigma_1| = |x_4 - \overline{x}_4|$ is monotonically decreasing [35], while the control signal u is time-varying but always satisfying $0 < u < 1$. Therefore, during the reaching phase, while the state x_4 converges in finite time to its reference $\overline{x}_4$ as proven above, the error variable Δx_d is treated as unknown but bounded. This is a conventional assumption in SM stability analysis [19].

Remark 5 (Equivalent Control): It is essential to note that in (29), the notion of equivalent control in SM control theory [19], [24] is used. The equivalent control $u_{\text{sm}}^{\text{eq}}$ does not correspond directly to the control signal u_{sm} applied to the SEPIC system. Instead, it can be seen as an average representation of the effect of discontinuous SM control on maintaining the system on the sliding surface (17). Therefore, our control scheme, as expressed in (17)–(20), only requires knowledge of the output voltage x_4.

Remark 6 (Analytical Expression of λ_1, λ_{23}): Note that an explicit representation of the eigenvalues of $M_d(\overline{u})$ can be determined. If $R_1 = R_2 = R$, $L_1 = L_2 = L$, $C_1 = C_2 = C$ are set, the three eigenvalues are

$$\lambda_1(\overline{u}) = -\frac{R}{L} \tag{58}$$

$$\lambda_{2,3}(\overline{u}) = -\frac{R}{2\,L} \pm \left(\frac{\sqrt{8L\overline{u}^2 - 8L\overline{u} + 4L - CR^2}}{2L\sqrt{C}}\right) j. \tag{59}$$

Remark 7 (Lossless Inductors Analysis): In extending the methodology presented in [8], our findings offer a broader perspective on the stability characteristics of the matrix $M_d(\overline{u})$. Specifically, when resistances R_1 and R_2 are eliminated ($R_1 = R_2 = 0$), yet with inductors and capacitors remaining unequal ($L_1 \neq L_2$, $C_1 \neq C_2$), the analysis yields the following eigenvalues:

$$\lambda_1(\overline{u}) = 0 \tag{60}$$

$$\lambda_{2,3}(\overline{u}) = \pm \left(\sqrt{\frac{(L_1 + L_2)\overline{u}^2 - 2L_2\overline{u} + L_2}{L_1L_2C_1}}\right) j. \tag{61}$$

These results corroborate the findings of [8], demonstrating that the system exhibits marginal stability with eigenvalues located on the imaginary axis. The derived eigenvalues, reflecting the zero dynamics of the system, are characterised by real parts equal to zero and distinct algebraic and geometric multiplicities, each being equal to 1. Applying linear control theory, as [8] have done, confirms that the system remains stable under the condition of zero resistances. It is crucial to note that the conclusions drawn in Proposition 1 (A) and (B) continue to apply even with the assumption of $R_1 = R_2 = 0$. This underscores the robustness of the stability characteristics of the system in the absence of resistive elements.

Remark 8 (Time-Varying Resistor R_L): The conducted stability analysis considered the load resistor R_L as an unspecified yet constant parameter, following a conventional approach [12], [22]. This was essential to guarantee the existence of the equilibrium (7)–(10). It is crucial to emphasise that the SOSM control scheme employed remains robust to variations in R_L. Specifically, when considering the time-dependent change of R_L, the term $-\dot{R}_L/R_L$ will be incorporated into (37). The influence of load fluctuations on the performance of output voltage regulation will be explored in the experimental tests of our study. The positive constant H defined in (38), which is required for the selection of controller parameters, can be chosen conservatively to account for the possible variations in R_L.

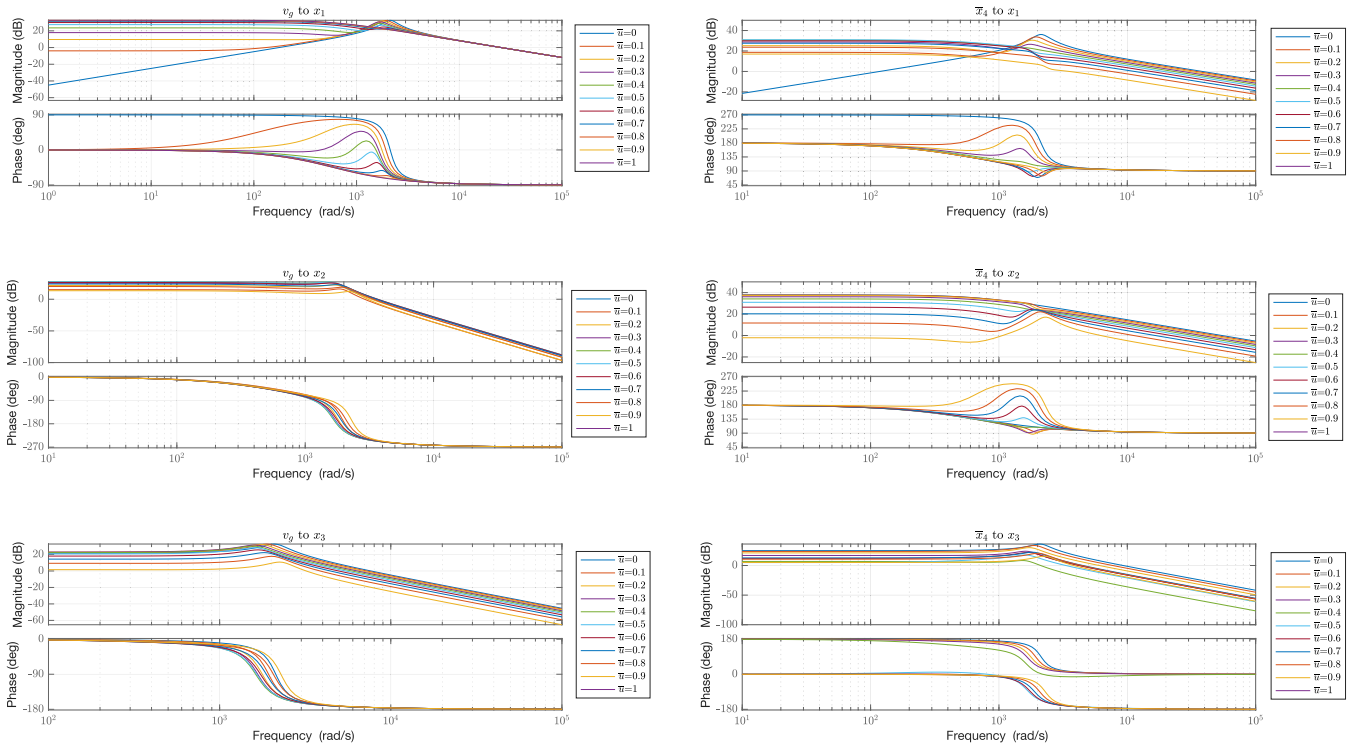

Fig. 3. Frequency response of the zero dynamics in (49), in the form of bode diagrams of magnitude and phase. The three states x_1, x_2, x_3 are analyzed. (Left): v_g is the considered input. (Right): $\overline{x}_4$ is the considered input. The zero dynamic is parameterized with respect to the duty cycle $\overline{u}$.

Remark 9 (Time-Varying SEPIC Parameters): The observation made in Remark 8 extends to situations where the parameters of the SEPIC converter vary over time. Importantly, variations in C_2 are the only factor that influences the 2-SOSM control strategy. A time-varying C_2 introduces the term $-\dot{C}_2/C_2$ into (37). Analogously, if the voltage reference $\overline{x}_4$ is time-varying, it will introduce the additional term $\ddot{\overline{x}}_4$ in (37). To maintain the integrity of the sliding mode, it is crucial to select the constant H in (38) with a conservative approach.

Frequency Analysis of the Zero Dynamics

It is important to analyse the frequency response of zero dynamics in (49). Given the model parameters reported in Fig. 1, the magnitude and phase bode diagrams are evaluated in the MATLAB environment, considering as input $p_d = [v_g,\, \overline{x}_4]^\top$, and as output the state vector $x_d = [x_1,\, x_2,\, x_3]^\top$. The results are depicted in Fig. 3. The plots are also parameterized with respect to the constant duty cycle $\overline{u}$. The identified bandwidth of closed-loop systems is on the order of 10^4 (rad/s). Furthermore, a damped resonance frequency is determined for the value 2000 (rad/s).

IV. Experimental Tests on an Embedded System Architecture

In this section, a series of conducted experiments are presented to confirm the theoretical main result of this paper using an embedded system architecture.

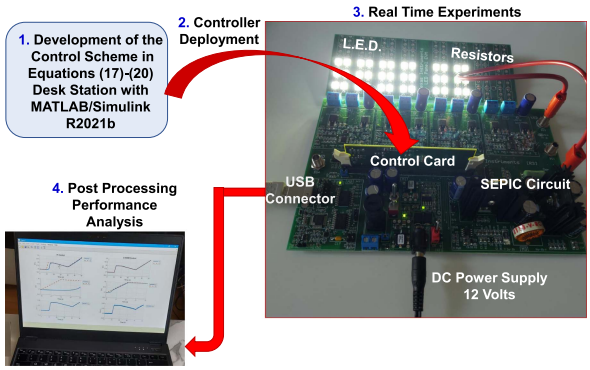

Fig. 4. Schematic of the embedded experiment methodology. The DC/DC LED lighting power board developed by Texas Instruments (TMDSDCDCLED-KIT) is interfaced with a MATLAB/Simulink R2021b environment where the control scheme is developed (step 1). The control scheme is then deployed on the Piccolo control card (step 2). After the execution of the experiments in the embedded architecture (step 3), the collected measurements are sent to a laptop to perform post-process analysis (step 4).

Setup Description and Controller Design: The experimental setup and is shown in Fig. 4. The equipment is composed of: a dc/dc LED lighting power board developed by Texas Instruments (*TMDDSDCDCLEDKIT*) [33], a *Piccolo F28069 ControlCard* [34], a load composed of an array of LEDs and resistors. The device is powered by a constant 12 Volt dc power adapter, plugged in the main grid (220 Volt AC, 50 Hz). Fig. 4 describes the underlying procedure that has been followed to carry out the experiments. The control algorithm was first

developed in a MATLAB-Simulink R2021b environment. The design constant for the proposed PWM-based 2-SOSM controller as in (18)–(20) is $\mu = 1$. This fixed value has been obtained by selecting $\alpha^\star = 0.5$, $G_1 = 1,000$, $G_2 = \frac{2.5}{500\times10^{-6}} = 5000$, $H = \frac{0.05}{500\times10^{-6}} = 100$ and solving the inequality (44), which yields $\mu = 1 > \max(0.04,\, 0.8)$. Once the 2-SOSM control scheme was proven successful and reliable in MATLAB simulation, the control algorithm was deployed on the Piccolo Controlcard and real-time experiments were executed. The hardware PWM modulation of the SEPIC has a sampling time of $T_d = 0.01$ ms (a PWM frequency of 100 kHz). Similar experimental sampling times have been chosen for the specific application of SEPIC in existing relevant works, such as [8] and [12] The approach is also supported by relevant theoretical results regarding the discretisation of SM control schemes using Euler's method [37]. The embedded system of the SEPIC includes a preexisting PI control already designed for the PWM modulation of the SEPIC [33]. The PI control variable is given by

$$u_{PI} = k_I \int \sigma d\tau + k_P \sigma \tag{62}$$

where $k_I = 0.0273$ and $k_P = 0.0018$. The output signal of the PI controller is saturated to ensure $0 < u_{PI} < 1$. The appropriate procedure adopted here provides a comparison of the existing PWM-based PI control strategy for SEPIC, which is already available for this device, with the 2-SOSM strategy proposed in this article. The aim is to demonstrate the performance enhancement that our methodology can guarantee when compared with the existing one.

Performance Metrics: The following three metrics are proposed to comprehensively evaluate the performances of the voltage regulation strategies

$$\mathcal{M}_{\text{av}} = \frac{1}{T}\int_0^T |\sigma| \tag{63}$$

$$\mathcal{M}_{\max} = \max(\sigma), \ \text{if}\, \exists\, t : \sigma(t) > 0 \tag{64}$$

$$\mathcal{M}_{\min} = \min(\sigma), \ \text{if}\, \exists\, t : \sigma(t) < 0 \tag{65}$$

where $\mathcal{M}_{\text{av}}$ accounts for the average tracking accuracy, $\mathcal{M}_{\max}$ captures the maximum overshoots of the sliding variable, if present, and $\mathcal{M}_{\min}$ captures the minimum overshoot of the sliding variable, if present. For each of the three introduced metrics, the reduction percentage is defined as

$$\Delta\mathcal{M}_{1-\text{SM}} := \frac{\mathcal{M}_\bullet^{1-\text{SM}} - \mathcal{M}_\bullet^{\text{PI}}}{\mathcal{M}_\bullet^{\text{PI}}}\ (\%), \tag{66}$$

$$\Delta\mathcal{M}_{2-\text{SOSM}} := \frac{\mathcal{M}_\bullet^{2-\text{SOSM}} - \mathcal{M}_\bullet^{\text{PI}}}{\mathcal{M}_\bullet^{\text{PI}}}\ (\%) \tag{67}$$

where $\mathcal{M}_\bullet^{\text{PI}}$ denotes one of the three metrics calculated using the PI control, $\mathcal{M}_\bullet^{1-\text{SM}}$ denotes one of the three metrics calculated using the 1-SM control, and $\mathcal{M}_\bullet^{2-\text{SOSM}}$ denotes one of the three metrics calculated using the proposed 2-SOSM control. The higher (in absolute value) $\Delta\mathcal{M}$, the better the considered control scheme performs compared to the PI control scheme.

TABLE II
VALUE OF THE PERFORMANCE METRICS ALONG WITH THE INDEX OF REDUCTION $\Delta\mathcal{M}$

	PI	1-SM	2-SOSM	$\Delta\mathcal{M}_{1-\text{SM}}$	$\Delta\mathcal{M}_{2-\text{SOSM}}$
$\mathcal{M}_{av}$	0.005	0.00020	0.00016	**-96%**	**-97%**
$\mathcal{M}_{\max}$	0.0473	0.0235	0.0194	**-50%**	**-59%**
$\mathcal{M}_{\min}$	-0.9945	-0.5458	-0.1356	**-45%**	**-86%**

Experimental Results: The following time-varying voltage reference profile:

$$\overline{x}_4(t) := \begin{cases} 17 & t \le 10 \\ 18 & 10 < t < 40 \\ 17.5 & t = 40 \\ 17.5 + 0.075(t-40) & 40 < t \le 60 \end{cases} \tag{68}$$

measured in Volts, is selected, as shown in Fig. 5. In the experimental analysis, the assumption that the voltage reference for the variable x_4 is always *constant* is relaxed, and, as per (68), periods of time where the reference is linearly time-varying are considered. Three scenarios are considered:

1) *Scenario PI*: the SEPIC is controlled via the PI controller (62)
2) *Scenario 1-SM*: the SEPIC is controlled via a 1-SM controller, which is governed by the control law

$$u_{1\text{SM}} = -0.5\text{sign}(\sigma). \tag{69}$$

3) *Scenario 2-SOSM*: the SEPIC is controlled via our 2-SOSM control scheme.

In all the three scenarios, the dynamic nature of a voltage reference is addressed, as defined by (68). Controlled variations in the load resistor R_L are introduced through an experimental setup involving automated switches governing an array of LEDs and resistors. The exercise is divided into three distinct time intervals, each contributing uniquely to the assessment of the sensitivity and robustness analysis of our scheme

1) In the initial interval (0–10 s), both the output voltage reference $\overline{x}_4$ and the load resistor R_L are held constant.
2) In the subsequent interval (10–40 s), the output voltage reference $\overline{x}_4(t)$ varies over time, while the load resistor R_L remains constant.
3) Finally, in the final interval (40–60 s), both the output voltage reference $\overline{x}_4(t)$ and the load resistor $R_L(t)$ undergo simultaneous time-varying changes.

The results of the experiments carried out are shown in Fig. 5 and Table II. In all the three scenarios maintaining the constancy of $\overline{x}_4$ and R_L yields highly accurate tracking of the reference. When $\overline{x}_4(t)$ is subject to variations while R_L remains constant, Scenario PI encounters challenges in reference tracking. In Scenario 1-SM the time-varying voltage reference is acceptably tracked, but the system is subject to a substantial chattering effect. Our proposed scheme in Scenario 2-SOSM ensures reliable tracking accuracy. Similar observations apply when both $\overline{x}_4$ and R_L undergo concurrent variations. The proposed 2-SOSM control strategy is praised for its improved precision throughout the experiment. As indicated in Table II,

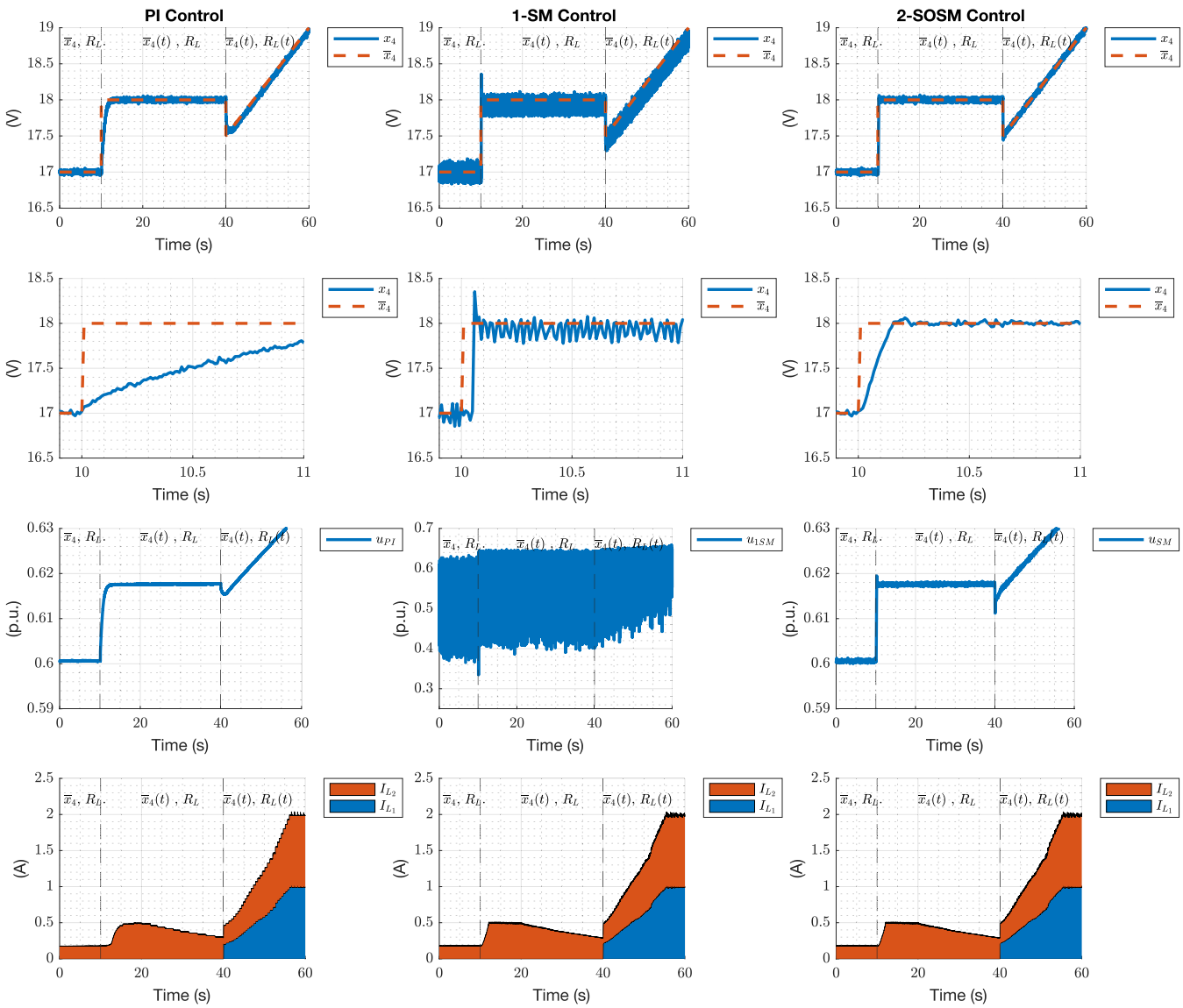

Fig. 5. *(Left):* Scenario PI; *(Centre):* Scenario 1-SM; *(Right):* Scenario 2-SOSM. From the top to the bottom: time histories of the SEPIC output voltage x_4 along with its reference value $\overline{x}_4(t)$, with an enlarged view during the time period $[10,\ 11]$ seconds, the control signals u_{PI}, $u_{1-\text{SM}}$ u_{SM}, and the currents I_{L_1}, I_{L_2} absorbed by the resistor arrays and LEDs.

our method shows an impressive improvement 97% in average tracking accuracy, a 59% reduction in overshoot, and a 86% decrease in undershoot. Collectively, these results highlight the effectiveness of the 2-SOSM strategy in significantly improving system performance. The data underscore not only the 2-SOSM capability to improve tracking precision, but also its potential to reduce unwanted transient behaviors. Although the 1-SM control strategy offers substantial performance enhancement compared to the PI control strategy, it is affected by a significant chattering effect. This effect causes the output voltage, denoted $x_4(t)$, to oscillate at high frequency. In conclusion, this study introduces significant advances in control methodology, particularly through the implementation of the 2-SOSM approach. This method provides promising opportunities for performance improvements in the SEPIC system.

Sensitivity Analysis of Scenario 2-SOSM

To evaluate the performance of the proposed control law (Scenario 2-SOSM) under more challenging conditions, we run a high-fidelity simulation in the MATLAB Simscape Electrical Environment and impose perturbations to the model parameters, namely inductors L_1, L_2, and capacitors C_1, C_2, and to the input voltage v_g. In these two analyses, the reference voltage profile is still governed by (68), and the load resistor R_L varies over time as above. Furthermore, the auxiliary variable $\tilde{\sigma}$ is introduced, which is defined according to (17), but in the situation when perturbations are present.

Model Parameters: The model parameters can vary over time for a number of factors that affect SEPIC, such as the ageing of the components, the temperature, and other external disturbances. Although such disturbances are present but unknown in

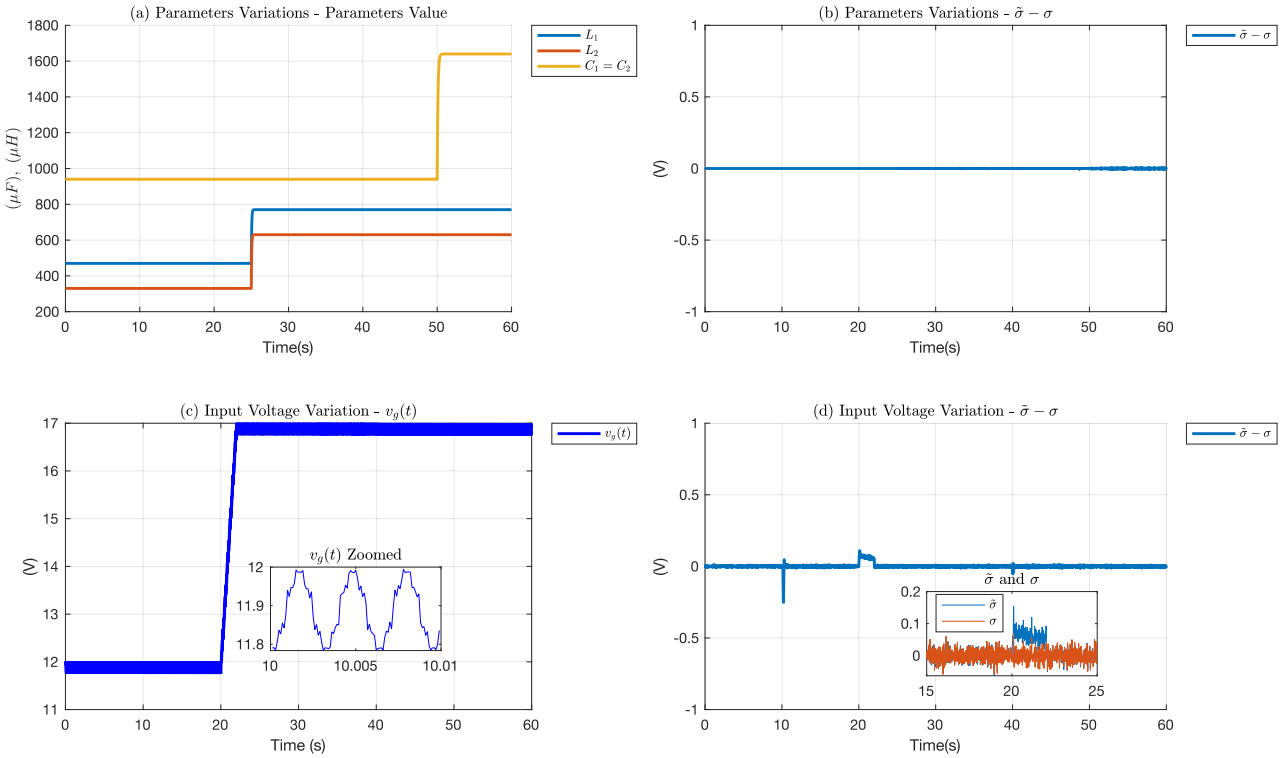

Fig. 6. Time histories of: (a) The time varying parameters; (b) The signal $\tilde{\sigma} - \sigma$; (c) The input voltage perturbation $v_g(t)$ with an enlarged view; (d) The signal $\tilde{\sigma} - \sigma$ with an enlarged view of both $\tilde{\sigma}$ and σ.

the experimental cases discussed above, it is possible to arbitrarily alter the parameters in the Simscape Electrical environment. In particular, the considered perturbations are in the form of an exponential transient, which is

$$p_i(t) = p_{i1} + (p_{i2} - p_{i1}) \left(1 - e^{-\frac{t - T_{pi}}{\tau_{pi}}}\right) \text{step}(t - T_{pi}) \quad (70)$$

where $p_i(t)$ is a generic time-varying model parameter, p_{i1} is its starting (nominal) value, p_{i2} is its new steady-state value after the transient, τ_{pi} is the exponential constant, step$(\cdot)$ represents the step function, and T_{pi} is the time instant at which the parameter $p_i(t)$ starts to vary. For the Scenario 2-SOSM, variations to the inductors L_1, L_2 starting at time instant $T_{P_l} = 25$ (s), and variations to the capacitors C_1, C_2, starting at time instant $T_{P_c} = 50$ (s) are considered. The initial values of the model parameters are given in Fig. 1, while the new steady-state values of the parameters are: $L_{12} = 780$, $L_{22} = 620$ (μH), $C_{12} = 1650$, $C_{22} = 1650$ (μH) The exponential constant is chosen as $\tau_{pc} = \tau_{pl} = 0.1$ (s) Fig. 6(a) and (b) shows on the left-hand side the time histories of the model parameters, while on the right-hand side the difference $\tilde{\sigma} - \sigma$ is evaluated and it remains equal to zero, signifying that the proposed controller is totally insensitive to model parameter variations.

Input Voltage: The input voltage $v_g(t)$ is perturbed according to

$$v_g(t) = 12 + 0.1\sin(2000t) + \psi(t) + \text{ramp}(t_s = 20,\ t_f = 22,\ m_r = 1) \quad (71)$$

where $\psi(t)$ is a band-limited noise contains harmonic frequencies of 2000 (rad/s), the signal ramp$(t_s = 20,\ t_f = 22,\ m_r = 1)$ denotes a ramp function, starting at time instant t_s (s), ending at time instant t_f (s), with a slope of m_r (V/s). It is very important to note that the frequency 2000 (rad/s) corresponds to the value of the resonant frequency identified in the analysis in Fig. 3. Fig. 6(c) and (d) shows on the left the time histories of the input voltage $v_g(t)$ governed by (71), while on the right there is a comparison between the value of σ in the presence and absence of perturbations to $v_g(t)$. It is interesting to note in Fig. 6(c) and (d), the difference $\tilde{\sigma} - \sigma$ that maps the impact of the voltage perturbation to the output voltage accuracy. The impact of the perturbation $0.1\sin(2000t) + \psi(t)$ on the regulation of the output voltage is rejected by the proposed controller. A small deviation can be observed at $\tilde{\sigma}$ when the ramp variation to $v_g(t)$ is enforced, but it remains within acceptable limits, in the order of 0.1 (V).

V. Conclusion

In this article, a PWM-based control scheme capable of regulating in finite time the output voltage of SEPICs has been presented. Inspired by the 2-SOSM control approach, the control scheme has been designed and its stability property theoretically analyzed. The proposed algorithm has been implemented in an embedded framework and numerically demonstrated the superiority of the voltage regulation performance obtained compared to the results ensured by a standard PI control scheme. A sensitivity analysis has also confirmed the excellent performances

of of the proposed techniques under parameters variations and input voltage perturbations. The key findings of the present research can be viewed as starting points for further developments. Possible future fundamental research can focus on the so-called optimal reach of the sliding manifold so that the finite-time voltage regulation can be made faster. Desirable future applied research directions of the present proposal will focus on the experimental testing of our control scheme for SEPICs applied to EV lithium-ion charging infrastructures or in zero-emission powertrains.

REFERENCES

[1] S. S. Khan and H. Wen, "A comprehensive review of fault diagnosis and tolerant control in DC-DC converters for DC microgrids," *IEEE Access*, vol. 9, pp. 80100–80127, 2021.

[2] J. Ferguson, M. Cucuzzella, and J. M. Scherpen, "Exponential stability and local ISS for DC networks," *IEEE Contr. Syst. Lett.*, vol. 5, no. 3, pp. 893–898, Jul. 2021.

[3] C. Rao, A. Hajjiah, M. A. El-Meligy, M. Sharaf, A. T. Soliman, and M. A. Mohamed, "A novel high-gain soft-switching DC-DC converter with improved p&o MPPT for photovoltaic applications," *IEEE Access*, vol. 9, pp. 58790–58806, 2021.

[4] S. Chakraborty, H.-N. Vu, M. M. Hasan, D.-D. Tran, M. E. Baghdadi, and O. Hegazy, "DC-DC converter topologies for electric vehicles, plug-in hybrid electric vehicles and fast charging stations: State of the art and future trends," *Energies*, vol. 12, no. 8, 2019, Art. no. 1569.

[5] F. Balsamo, C. Capasso, D. Lauria, and O. Veneri, "Optimal design and energy management of hybrid storage systems for marine propulsion applications," *Appl. Energy*, vol. 278, 2020, Art. no. 115629.

[6] F. L. Luo and H. Ye, *Advanced DC-DC Converters*. Boca Raton, FL, USA: CRC Press, 2016.

[7] Y. Han, *Modeling and Control of Power Electronic Converters for Microgrid Applications*. Berlin, Germany: Springer, 2021.

[8] E. Garza-Arias, J. C. Mayo-Maldonado, J. E. Valdez-Resendiz, G. Escobar, J. Rosas-Caro, and D. Guillen, "Direct output-voltage control of non-minimum phase higher-order DC-DC converters," *IEEE Trans. Ind. Electron.*, vol. 70, no. 7, pp. 1455–1466, Feb. 2023.

[9] S. Hasanpour, T. Nouri, F. Blaabjerg, and Y. P. Siwakoti, "High step-up SEPIC-based trans-inverse DC–DC converter with quasi-resonance operation for renewable energy applications," *IEEE Trans. Ind. Electron.*, vol. 70, no. 1, pp. 485–497, Jan. 2023.

[10] L. Mo, Y. Wang, C. Jiang, X. Wang, and B. Zhang, "A novel topology derivation method revealed from classical cuk, sepic, and zeta converters," *IEEE Trans. Power Electron.*, vol. 39, no. 7, pp. 7828–7833, Jul. 2024.

[11] A. Sel, U. Güneş, and C. Kasnakoğlu, "Design of output feedback sliding mode controller for SEPIC converter for robustness," *Int. J. Electron.*, vol. 107, no. 2, pp. 239–249, 2020.

[12] H. Komurcugil, S. Biricik, and N. Guler, "Indirect sliding mode control for DC–DC SEPIC converters," *IEEE Trans. Ind. Inform.*, vol. 16, no. 6, pp. 4099–4108, Jun. 2020.

[13] N. Guler, S. Biricik, S. Bayhan, and H. Komurcugil, "Model predictive control of DC–DC SEPIC converters with autotuning weighting factor," *IEEE Trans. Ind. Electron.*, vol. 68, no. 10, pp. 9433–9443, Oct. 2021.

[14] S. Mouslim et al., "Simulation and analyses of SEPIC converter using linear PID and fuzzy logic controller," *Materials Today: Proc.*, vol. 27, pp. 3199–3208, 2020.

[15] M. Espinosa et al., "Passivity based-control of output voltage regulation with MPPT for photovoltaic panel using two sepic converters," in *Proc. IEEE Int. Autumn Meeting Power Electron. Comput.*, Ixtapa, Guerrero, Mexico, 2020, pp. 1–6.

[16] V. Mihaly, M. Şuşcă, D. Morar, and P. Dobra, "Sensitivity analysis of krasovskii passivity-based controllers," *Mathematics*, vol. 10, no. 20, 2022, Art. no. 3750.

[17] G. Rinaldi, P. P. Menon, C. Edwards, A. Ferrara, and Y. Shtessel, "Adaptive dual-layer super-twisting sliding mode observers to reconstruct and mitigate disturbances and communication attacks in power networks," *Automatica*, vol. 129, 2021, Art. no. 109656.

[18] V. Utkin, "Sliding mode control of DC/DC converters," *J. Franklin Inst.*, vol. 350, no. 8, pp. 2146–2165, 2013.

[19] A. Ferrara, G. P. Incremona, and M. Cucuzzella, *Advanced and Optimization Based Sliding Mode Control: Theory and Applications*. Philadelphia, PA, USA: SIAM, 2019.

[20] S. K. Pandey, S. Patil, S. Phadke, and A. Deshpande, "Investigation of sliding mode control of higher order DC-DC converters," in *Proc. IEEE 7th India Int. Conf. Power Electron.*, Patiala, India, 2016, pp. 1–5.

[21] G. Ablay, "Robust tracking controller for SEPIC drivers," *Electron. Lett.*, vol. 52, no. 24, pp. 2007–2009, 2016.

[22] M. Cucuzzella, R. Lazzari, S. Trip, S. Rosti, C. Sandroni, and A. Ferrara, "Sliding mode voltage control of boost converters in DC microgrids," *Control Eng. Pract.*, vol. 73, pp. 161–170, 2018.

[23] A. Levant, "Chattering analysis," *IEEE Trans. Autom. Control*, vol. 55, no. 6, pp. 1380–1389, Jun. 2010.

[24] Y. Shtessel et al. *Sliding Mode Control and Observation*. Berlin, Germany: Springer, 2014.

[25] S.-C. Tan, Y.-M. Lai, and K. T. Chi, "General design issues of sliding-mode controllers in DC–DC converters," *IEEE Trans. Ind. Electron.*, vol. 55, no. 3, pp. 1160–1174, Mar. 2008.

[26] B. A. Martinez-Trevino, A. El Aroudi, A. Cid-Pastor, G. Garcia, and L. Martinez-Salamero, "Synthesis of constant power loads using switching converters under sliding-mode control," *IEEE Trans. Circuits Syst. I: Regular Papers*, vol. 68, no. 1, pp. 524–535, Jan. 2021.

[27] H. Sira-Ramírez, "A geometric approach to pulse-width modulated control in nonlinear dynamical systems," *IEEE Trans. Autom. Control*, vol. 34, no. 2, pp. 184–187, Feb. 1989.

[28] Y. Cheng, G. Wen, and H. Du, "Design of robust discretized sliding mode controller: Analysis and application to buck converters," *IEEE Trans. Ind. Electron.*, vol. 67, no. 12, pp. 10672–10681, Dec. 2020.

[29] E. Mamarelis, G. Petrone, and G. Spagnuolo, "Design of a sliding-mode-controlled SEPIC for PV MPPT applications," *IEEE Trans. Ind. Electron.*, vol. 61, no. 7, pp. 3387–3398, Jul. 2014.

[30] A. Goudarzian, A. Khosravi, and H. A. Raeisi, "A new approach in design of sliding-mode voltage-controller for a SEPIC," *Int. J. Dyn. Control*, vol. 9, no. 3, pp. 1197–1209, 2021.

[31] V. Subramanian and S. Manimaran, "Implementation of a sliding mode controller for single ended primary inductor converter," *J. Power Electron.*, vol. 15, no. 1, pp. 39–53, 2015.

[32] G. Gireesh and P. Seema, "High frequency sepic converter with pwm integral sliding mode control," in *Proc. Int. Conf. Technological Advancements Power Energy*, 2015, pp. 393–397.

[33] V. Lenzi, "Developing DC-DC converter control in simulink," Matworks, Boston, MA, USS, Tech. Rep. 1, 2023.

[34] B. Larimore, "LED lighting and DC-DC conversion control integrated on one C2000 microcontroller," Texas Instruments Kit Documentation, Dallas, Texas, Tech. Rep. 1, 2010.

[35] A. Ferrara and M. Rubagotti, "A sub-optimal second order sliding mode controller for systems with saturating actuators," *IEEE Trans. Autom. Control*, vol. 54, no. 5, pp. 1082–1087, May 2009.

[36] J. Falin, "Designing DC/DC converters based on SEPIC topology," *Analog Appl.*, vol. 1, pp. 19–20, 2008.

[37] S. Li, H. Du, and X. Yu, "Discrete-time terminal sliding mode control systems based on euler's discretization," *IEEE Trans. Autom. Control*, vol. 59, no. 2, pp. 546–552, Feb. 2014.

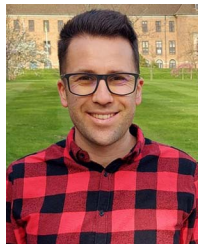

Gianmario Rinaldi received the B.Sc. degree in energy engineering, the M.Sc. degree in electrical engineering, and the Ph.D. degree in control systems engineering from the University of Pavia, Pavia, Italy, in 2014, 2016, and 2019, respectively.

He is currently a Lecturer in mechanical engineering with the Department of Engineering, Faculty of Environment, Science and Economy (ESE), University of Exeter, U.K. His expertise is in estimation, optimisation, clean mobility, and energy networks. He is the author of more than 20 peer-reviewed papers in these areas, including more than 15 journal publications.

Prathyush P Menon received the B.Tech. degree in electrical and electronics engineering from Mahatma Gandhi University, Kottayam, India, in 1997, the M.Tech. degree in aerospace engineering from the Indian Institute of Technology, Mumbai, India, in 2003, and the Ph.D. degree in control engineering from the Department of Engineering, University of Leicester, Leicester, U.K., in 2007.

He is an Associate Professor of control and autonomy with the Department of Engineering, Faculty of Environment, Science, and Economy. He leads the research activities in the Cooperative Robotics and Autonomous NEtworks (CRANE) lab. He is the author and co-author of more than 100 refereed papers in these areas, including 60 journal publications. His research interests include control, autonomy, multiagent systems, autonomy, sliding mode observers, energy networks, optimisation, simulation-based robustness analysis and uncertainty quantification.

Antonella Ferrara (Fellow, IEEE) received the M.Sc. degree in electronic engineering and the Ph.D. degree in computer science and electronics from the University of Genoa, Genoa, Italy, in 1987 and 1992, respectively.

Since 2005, she has been Full Professor of automatic control with the University of Pavia, Italy. She is author and co-author of more than 450 publications including more than 160 journal papers, two monographs and one edited book. She is/was Senior Editor and Associate Editor of the major scientific journals in the field of Automatic Control. She is currently an Associated Editor of *Automatica* and Senior Editor of the IEEE Open Journal of Intelligent Transportation Systems. Her main research interests are focused on nonlinear control, with a special emphasis on sliding mode control, applied to road traffic systems, automotive systems, power networks, and robotics.

Dr. Ferrara is the EUCA Conference Editorial Board Chair. She is a member of the IEEE TC on Variable Structure Systems, IEEE TC on Automotive Control, IEEE TC on Smart Cities, IFAC Technical Committee on Nonlinear Control Systems, IFAC TC on Transportation Systems, and IFAC Technical Committee on Intelligent Autonomous Vehicles. Among several awards, she was a co-recipient of the 2020 IEEE Transactions on Control Systems Technology Outstanding Paper Award. She is IFAC Fellow.